Tenth International Conference on Computational Fluid Dynamics (ICCFD10), Barcelona, Spain, July 9-13, 2018

ICCFD10-131

Simulation of Flow Fields around Complex Rotorcraft Configurations with a Fast, Two Layer Trim Model and Adaptive Embedded Grid

Ye Liang*, Yang Shuo*, Qi Shuni*, Dong Jun*
Corresponding author:yeliang1981@163.com

AVIC Aerodynamics Research Institute, China.

Abstract: Based on adaptive embedded grid system, the unsteady flow around complex rotorcraft configurations was simulated by Navier-Stokes equations. A two-layer trim model which composed by tilt actuator and unsteady aerodynamic calculation was developed for predicting the movement of rotors and blades, results obtained by tilt actuator model were used as initial guess for unsteady flow fields simulation. Three-dimensional unsteady Navier-Stokes equations were discretized by a second-order upwind finite-volume scheme and LU-SGS time-stepping scheme. The adaptive Cartesian grid, which was used as background grid for vortices capture, refined with the flow solution, and the actuator disk and blade body-fitted grids were used as minor grid respectively for the two different layer simulation. Solution processes for flow fields simulation, which were not for the equations discretisation iterations, but the grid assembly were speeded up by introduction of parallel method. With these methods, the flow fields of a tilt rotor configuration in conversion mode and a coaxial rotor in forward flight were simulated. Aerodynamic results show that better trimmed initial value can be obtained with the tilt actuator model under less computational efforts as the model's natural quasi-steady attribution, convergence acquired with almost 1-2 trim iterations for blades body-fitted grid simulation with this input and high computational efficiency was achieved.

Keywords: Rotorcraft, Two layer trim model, Unsteady, Actuator, Navier-Stokes equations.

1 Introduction

Rotorcraft trimming is setting control inputs for required flight conditions. The control inputs, for example, the shaft, collective and cyclic pitch angle etc, are not be specified directly but by solved with numerical method, so as to make the aerodynamic results satisfy the prescribed aircraft overall thrust, rolling and pitching moments. The precision of the predicted rotor aerodynamic is directly determined by the accuracy of rotor control inputs. Generally, a completely trimming loop includes aerodynamic simulation and trimming iteration process, the total amount of calculation is proportional to the production of rotor aerodynamic simulation costs and the number of trimming iterations.

Lots of rotor trimming researches can be retrieved in previous rotor aerodynamic simulation. Peters et al.[1] offered a general theory of rotorcraft trim which is not tied to any particular trim algorithm, it is exercised with periodic shooting to show how free-flying rotorcraft can be trimmed in a variety of ways by use of general theory. In respect of trimming algorithm researching, Sekhar et al.[2] investigated the basin of attraction for Newton–Raphson method used for helicopter trim, they found that the collective, lateral and longitudinal cyclic pitch of the main rotor are dominant variables

for helicopter coupled trim with restrictive basins of attraction. Gouravaraju[3] extended the studies of Chandrasekhar and Ganguli by investigating the basin of attraction for a particular case of lateral cyclic and longitudinal cyclic pitch in a quantitative manner. Dai et al.[4] improved the rotor trimming by the introduction of genetic algorithm, which has several advantages such as global convergence and mass searing. Enns et al.[5] developed a neural network-based approximate dynamic programming control mechanism which can be applied to complex control problems such as helicopter flight control design. Subramanian et al.[6] gave a parallel shooting method based on fast-Floquet theory and damped Newton iteration to predict helicopter trim. Some studies[7,8] shows that at least 4-10 trimming iterations are needed for obtaining the convergence control variable inputs for such a typical nonlinear systems, the flow solver need to be called for one or several times owing to different trimming algorithm in order to estimate the aerodynamic or it's derivative in each iteration. The researchers also need to choose a reasonable aerodynamics model in order to make the calculation amount in a controllable range. Due to the limitation of computing ability, earlier rotor trimming calculation adopts dynamic inflow model to estimate the aerodynamic of rotor[9], the actuator disk method[10,11] is also used by some researchers, precision of the predicted thrust and moments are limited since the simplified aerodynamic distributions and time averaged formulation deduced from the simplified or blade element theory cannot properly simulate the unsteady flow over blades. Steijl et al.[12] introduced the unsteady CFD model for aerodynamic calculation, Zhong et al.[13] introduced the hybrid aerodynamics model to improve the accuracy of the aerodynamic results. In recent years, the trimming calculation of some rotors with complex configuration had also been carried out, for example, literature [14] gave a research on trimming a ABC rotor with 7 variables. It can be found in most previous studies, simplified aerodynamics model for control input calculation was adopted, the precision of the overall trimming calculation is limited by the computing resource restriction. In addition, in order to cut the consumption of time and resource, unsteady aerodynamic force was calculated by directly using trimming results which generated by a lower-order CFD research trimming process as a control input in some research works, the lack of coupling iterations also reduced accuracy of rotor CFD.

As the improvement of computer hardware and the wide application of large-scale parallel computing technology, the rotor CFD technology is developing by leaps and bounds. The rotorcraft aerodynamic simulations with some high precision numerical model has become possible, but as the trimming calculation is an iterative process, the flow solver must be called repeatedly, there still need effective strategies to control the size of simulation and speed up calculation .

In view of this, the following research work was conducted: A two-layer trim model was developed by combining two separated trimming process, the Newton iteration was used to trim the lift, drag and moment in both the two stage, only with aerodynamic model differences. The tilt momentum source model was adopted in first trimming step for aerodynamic and Jacobin matrix (The partial derivative of aerodynamic with respect to control inputs) estimation, several iterations are needed for an appropriate solve, the calculation amounts were not large, as the grid numbers can be saved with the actuator simplification and no blade configuration and real movements described, the each flow fields calculation is also economical for the natural quasi-steady characteristics of momentum source method. Then the control variables generated from the first step was used as initial guess to initialize the unsteady flow fields with blade body-fitted embedded grid for the second trim stage, a fast trim convergence rate is observed with numerical experiments, only 1-2 Newton iterations are needed for obtaining the ultimate convergence results, the total consumption can be endured due to the reduction of Newton iteration numbers, although the much computational efforts are still needed with unsteady Navier-Stokes solver calling. With this characteristics, more refined grid can be used in trimming iterations, and better trimming results are anticipated to be obtained. The embedded grid system which was composed by a background and several minor grid blocks, was adopted for rotorcraft CFD simulation. The adaptive Cartesian background grid, which was a rather sparse one at first, can be refined with grid pre-assembly feedback and flow solution gradient after several flow field iterations gradually, which make the flow details (vorticity and separation) capture possible with a high quantity of grid cells distribution. The actuator disk and blade body-fitted grid blocks were used as minor grid respectively for the two different trimming stage, the tilt matrix was appended to the overall coordinate system conversion matrix to realized the large shaft angle simulation, which is important for a rotorcraft with complex configuration or work state(such as a tilt

rotor).Three-dimensional Navier-Stokes equations were discretized by a second-order upwind finite-volume and LU-SGS time-stepping scheme. A dual time stepping method was used for unsteady flow fields simulation. The one equation Spalart-Allmaras model was used for eddy estimation. Solution processes for flow fields simulation, which were not for the equations discretisation iterations, but the grid assembly were speeded up by introduction of MPI based parallel method, which further shorten the time consumption of total trimming calculation.

Based on the above mentioned method, A tilt rotor and coaxial rotor in wind tunnel test state are simulated, the control variables contain not only the collective angel, but cyclic and rotor shaft angle. The calculation results showed that the presented method has better convergence and time efficiency for the rotor trimming, and suitable for the aerodynamic calculation of complex configuration rotor.

2 Grid system

2.1 Unstructured/Cartesian adaptive overset grid

Embedded grid system is selected to avoid grid regeneration as the relative movement (blade flapping and pitching) exists among the moving bodies. The whole grid system is composed of background and body-fitted grids[15]. Hexahedron cell is selected to fill the region near the blade where the viscosity phenomenon must be considered to maintain the grid quality. The Cartesian grid is selected as the background grid, which is generated and refined for the first time by grid assembly result and pre-described blade (actuator) movement input, the refine work can also be repeated for several times with flow fields iterations based on characteristic variables gradient and grid assembly. The body-fitted and Cartesian grid block are all stored as an unstructured format to unify the numerical scheme for flow solver.

2.2 Grid assembly method

Configuration for "hole" in embedded grid is described by the grid lines around the body surface. An auxiliary structured grid with a specified resolution is generated to define the "hole" and accelerate the "hole cutting" process by replacing the cell "in or out" judgment with simple coordinate comparison.

In “donor searching” step, Another auxiliary structured grid was generated for primary donor localization, after this, a Neighbor to Neighbor method is adopted to identify the exact donor. Donor searching is only limited to several cells around the "hole" and out boundary cells of minor grid blocks.

3 Two-layer trim model

The trim equations are solved with Newton iteration. In the first step, the rotor aerodynamic are estimated by actuator model, then unsteady flow fields are initialized with the trimmed blade movement results obtained from the first step as initial guess, and the revised trimming results are brought out eventually with another several iterations. The Newton iteration can be written as

$$\begin{bmatrix} C_{FX}{}^{tar} - C_{Fx} \\ C_{FY}{}^{tar} - C_{FY} \\ C_{FZ}{}^{tar} - C_{FZ} \\ C_{MX}{}^{tar} - C_{Mx} \\ C_{MY}{}^{tar} - C_{MY} \\ C_{MZ}{}^{tar} - C_{MZ} \end{bmatrix} = \begin{bmatrix} \frac{\partial(C_{FX})}{\partial(\upsilon 1)} & \frac{\partial(C_{FX})}{\partial(\upsilon 2)} & \frac{\partial(C_{FX})}{\partial(\upsilon 3)} & \frac{\partial(C_{FX})}{\partial(\upsilon 4)} & \frac{\partial(C_{FX})}{\partial(\upsilon 5)} & \frac{\partial(C_{FX})}{\partial(\upsilon 6)} \\ \frac{\partial(C_{FY})}{\partial(\upsilon 1)} & \frac{\partial(C_{FY})}{\partial(\upsilon 2)} & \frac{\partial(C_{FY})}{\partial(\upsilon 3)} & \frac{\partial(C_{FY})}{\partial(\upsilon 4)} & \frac{\partial(C_{FY})}{\partial(\upsilon 5)} & \frac{\partial(C_{FY})}{\partial(\upsilon 6)} \\ \frac{\partial(C_{FZ})}{\partial(\upsilon 1)} & \frac{\partial(C_{FZ})}{\partial(\upsilon 2)} & \frac{\partial(C_{FZ})}{\partial(\upsilon 3)} & \frac{\partial(C_{FZ})}{\partial(\upsilon 4)} & \frac{\partial(C_{FZ})}{\partial(\upsilon 5)} & \frac{\partial(C_{FZ})}{\partial(\upsilon 6)} \\ \frac{\partial(C_{MX})}{\partial(\upsilon 1)} & \frac{\partial(C_{MX})}{\partial(\upsilon 2)} & \frac{\partial(C_{MX})}{\partial(\upsilon 3)} & \frac{\partial(C_{MX})}{\partial(\upsilon 4)} & \frac{\partial(C_{MX})}{\partial(\upsilon 5)} & \frac{\partial(C_{MX})}{\partial(\upsilon 6)} \\ \frac{\partial(C_{MY})}{\partial(\upsilon 1)} & \frac{\partial(C_{MY})}{\partial(\upsilon 2)} & \frac{\partial(C_{MY})}{\partial(\upsilon 3)} & \frac{\partial(C_{MY})}{\partial(\upsilon 4)} & \frac{\partial(C_{MY})}{\partial(\upsilon 5)} & \frac{\partial(C_{MY})}{\partial(\upsilon 6)} \\ \frac{\partial(C_{MZ})}{\partial(\upsilon 1)} & \frac{\partial(C_{MZ})}{\partial(\upsilon 2)} & \frac{\partial(C_{MZ})}{\partial(\upsilon 3)} & \frac{\partial(C_{MZ})}{\partial(\upsilon 4)} & \frac{\partial(C_{MZ})}{\partial(\upsilon 5)} & \frac{\partial(C_{MZ})}{\partial(\upsilon 6)} \end{bmatrix} \begin{bmatrix} \Delta\upsilon 1 \\ \Delta\upsilon 2 \\ \Delta\upsilon 3 \\ \Delta\upsilon 4 \\ \Delta\upsilon 5 \\ \Delta\upsilon 6 \end{bmatrix}$$

Where C_{FX}, C_{FY}, C_{FZ}, C_{MX}, C_{MY}, C_{MZ} is the force and moment for balance evaluation, "tar" means target, $\Delta\upsilon 1 \sim \Delta\upsilon 6$ is undetermined increments of trimming variables. The partial derivative of aerodynamic with respect to trimming variables in Jacobin matrix is solved by dividing the aerodynamic augmenter by the corresponding tiny increment of the trimming variables. The flow

solver was called for N+1 times for one trimming iteration, where N is the numbers of undetermined trimming variables, another call is used for force and moment evaluation for the equation left hand terms.

4 Control equations and numerical method

4.1 Navier-Stokes equations

The 3D Reynolds-averaged Navier-Stokes equations can be written in an integral form for a moving control volume Ω with a surface element dS:

$$\frac{\partial}{\partial t}\iiint_{\Omega}\vec{W}d\Omega+\iint_{\partial\Omega}(\vec{F_c}-\vec{F_v})dS=\int_{\Omega}\vec{Q}\,d\Omega$$

Where$\vec{W}$ is conservative variables, $\vec{F_c}$ represents convective flux vector, $\vec{F_v}$ is the vector of the v iscous fluxes, $\vec{Q}$ represents source term, which can be evaluated as an appended momentum when the rotor was treated as an actuator, will be discussed next. For a cell-centered scheme, the flow variables are stored at the centre of the grid cells.

4.2 Tilt momentum source

For an actuator model[16], rotor was treated as an infinite thin disk, and the blade configuration is not considered. In order to describe the rotor shaft angel variation in trimming process conveniently, several minor grid blocks, each only contains a single actuator disk for rotor describing, is adopted as minor grids and embedded in the background grid.

The actuator disk is discretized into small elements, For a tiny element on the plane of actuator disk, the area is S_Δ, the distance from the center of hub is r, with a length of dr along the spanwise direction. Supposing that the force acting on the blade is $d\vec{F}$, the time averaged force on the grid cell surface is $\frac{NS_\Delta(-d\vec{F})}{2\pi rdr}$(N is the blade numbers).

The force acting on the blade $d\vec{F}$, can be calculated in rotor reference coordinate (ξ,η,ζ) where forces along ξ and η direction are left and the forces along the span (ζ direction) are neglected, the sectional forces can be obtained by consulting the table of aerodynamic force coefficients of 2D aerofoil. The forces in ξ and η direction can be written as

$$f_{\Delta\xi}=\frac{N(-dF_\xi)S_\Delta}{2\pi rdr}=\frac{-N(-dL\sin\alpha+dD\cos\alpha)S_\Delta}{2\pi rdr}$$

$$f_{\Delta\eta}=\frac{N(-dF_\eta)S_\Delta}{2\pi rdr}=\frac{-N(dL\cos\alpha+dD\sin\alpha)S_\Delta}{2\pi rdr}$$

The attack angle α for the airfoil, is decided by inflow in (ξ,η) direction, which is calculated from velocity in inertial coordinate by transformation, and the blade sectional forces in rotor reference coordinate are needed to be transformed back to inertial coordinate to finish the source appending.

For a rotor with shaft angle, coordinate transformation between inertial and rotor reference frame can be written as following, where M1,M2,M3,M4 is tilt, rotation, flap, pitch matrix of the blade[17].

$$\begin{bmatrix}(x-x_{nrc})\\(y-y_{nrc})\\(z-z_{nrc})\end{bmatrix}=[M1][M2][M3][M4]\begin{bmatrix}\xi-\xi_{rrc}\\\eta-\eta_{rrc}\\\zeta-\zeta_{rrc}\end{bmatrix}+[M1]\begin{bmatrix}\xi\xi_{rrc}-\xi\xi_{nrc}\\\eta\eta_{rrc}-\eta\eta_{nrc}\\\zeta\zeta_{rrc}-\zeta\zeta_{nrc}\end{bmatrix}$$

4.3 Numerical scheme

Dual time-stepping approach is used for unsteady flows simulation when the blade body fitted grid is used. Define that m is the pseudo-time, n is the physical time, the equations can be written as[18]:

$$\left\{\frac{V_i}{\Delta\tau}+\frac{3V_i}{2\Delta t}-\left[\frac{\partial\vec{R}}{\partial\vec{W}^*}\right]^m\right\}\Delta\vec{W}^*=\frac{3\vec{W}^*-4\vec{W}^n+\vec{W}^{n-1}}{2\Delta t}V_i+\vec{R}^m(\vec{W}^*)$$

Where, V_i is the volume of control unit, $\Delta\tau$, Δt , are pseudo and physical time step, and $\vec{R}^m$ is the residual after the n^{th} iteration in physical time domain. The solution is marched forward to the steady s tate in pseudo time domain through a LU-SGS[19] iteration. For the actuator model, the flow field is q uasi-steady, the dual time-stepping approach was not launched.

Second-order accuracy of ROE's scheme[20] can be derived by using solution reconstruction algorithm, which is used for convective flux calculation. Gradient of variables can be calculated with

the Guass-Green law. The Venkatakrishnan limiter functions[21] are adopted to avoid generating new extrema in high gradients regions for its superior convergence properties. The Spalart-Allmaras turbulence model[22] is selected to estimate the eddy viscosity, the turbulence equation is also be solved with LU-SGS iteration.

4.4 Parallelization

For a distributed memory system, domain decomposition is executed to subdivide each grid block in the unstructured/Cartesian embedded grid system into equal size sub-domains, each sub-domain which belongs to a grid blocks is assigned to different processor so that all threads can work on their own sub-domain in parallel.

Except the input, output module with nature of data dependency is executed with master thread only, most portions of the code are parallelized, not including the flow solver but the grid assembly module. The LU-SGS time marching need to be modified to fit the distributed memory system, the parallel "hole cutting" is achieved by broadcasting hole construction sub-grid surface to all processors, and an additional data communication among different processors is implemented to realize the parallel "donor searching", as each component grid is attached to some moving object, the cells position in one grid blocks needs to be communicated with the corresponding messages in other processors.

The computational domain needs to be repartitioned after each background grid adaptation to achieve the load balance.

5 Results and discussions

5.1 Validation cases for aerodynamic calculation

5.11 Dynamic pressure calculations on an experimental rotor

In order to validate the ability of actuator model, a model rotor in hover state is adopted for flow field dynamic pressure calculation. The rotor is composed by two untwisted and untapered blades, the radius is 0.914m, the chord length is 0.1m, M_{tip} in hover is 0.3285, the collective angle is 11°. Figure 1 is comparison of predicted dynamic pressure distributions with experimental data[23] at different axial (Y=0.215,0.325) positions, the calculated results shows a good agreement with the experimental data.

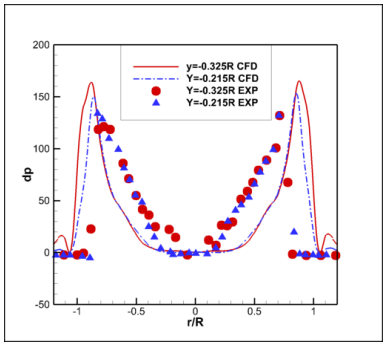

Figure 1: Comparisons of predicted dynamic pressure distributions with experimental data

5.12 Induced velocity calculation on a coaxial rotor in hover

An experimental coaxial rotor[24] in hover state is used as the second validation case, the rotor is composed by a upper and lower rotor with a distance 0.175m in vertical direction. The radius of the two rotor are 0.945m, the rotor blades are non-twisted, with the root chord 0.175m and an taper from the 0.95R to tip, taper ratio is 1/3, the section airfoil is NACA0012. The collective angle setting is 9 and 10.27 degrees respectively for torque balance, M_{tip} in hover is 0.347. The actuator model was used for numerical simulation. Figure 2 gives the predicted induced velocity distributions in three different directions beneath the rotor, which show good agreement with experimental data for axial velocity, the radial velocity difference is a little larger, as the force in this direction is neglected with momentum source model, the induced velocity in circumferential direction, is a rather small value and not be discussed here.

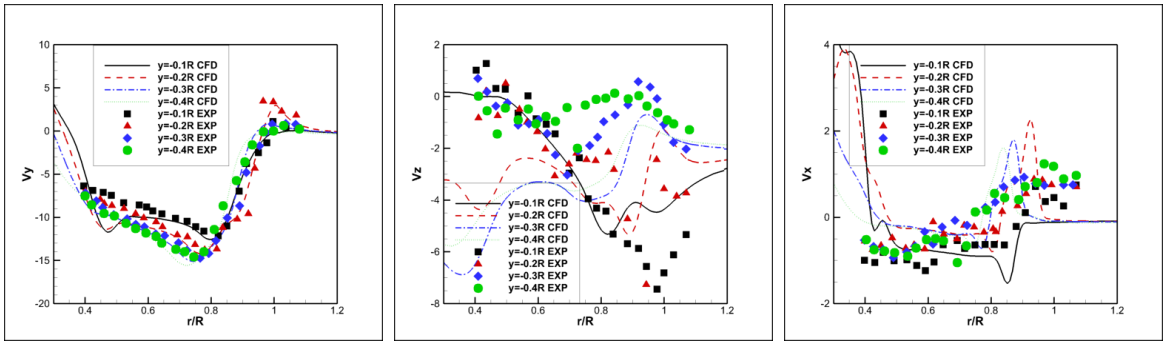

(a) axial (b) radial (c) circumferential

Figure 2: Comparisons of predicted induced velocity beneath a coaxial rotor with experimental data

5.13 Rotor/fuselage interaction calculation based on body-fitted based grid

The 'Georgia-Tech rotor' geometry[25] in forward flight is adopted as the third validation case. It has a 2-bladed rotor and a cylinder fuselage, the blades have NACA0015 aerofoil sections and rectangular plane form, the chord length is 0.0086m, with no geometric twist and taper, the radius of the rotor is 0.4572m, the rotational speed is 2100rpm and the advanced ratio is 0.2. Flap coefficients are $\beta_{1c} = -3.39$ and $\beta_{1s} = -2.62$ with the collective angle 10° and shaft angle 6°. The tetrahedron cell is selected for background grid. The body fitted grid is used for describing the blade configuration and movement, the unsteady flow field and aerodynamic is solved. Figure 3 shows flow field and aerodynamic for this test case. The agreements among calculation and experimental data are good for the time averaged pressure along the fuselage crown line.

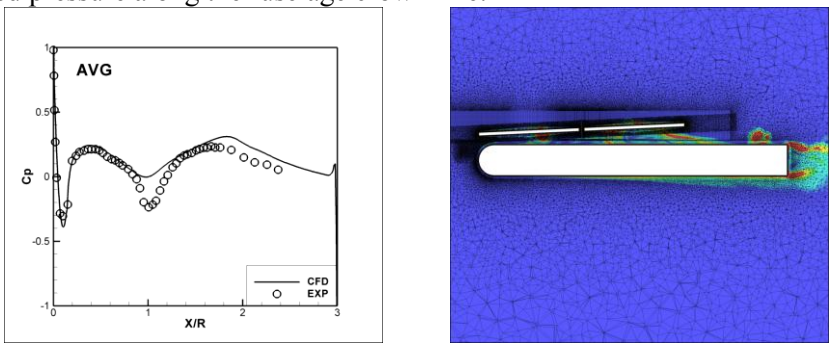

Figure 3: Aerodynamic and flow fields for ' Georgia-Tech rotor ' geometry in forward flight

5.2 Validation cases for trimming a single rotor

The test cases involve two forward flight trimming processes of a 2-bladed rotor[26]. The rotor blades are untapered, non-twisted with an aspect ratio of 6 and have a symmetric NACA0012 profile. For these cases, M_{tip}=0.439, advanced ratio is 0.268.

5.21 Convergence comparison of trim iteration with different Jacobin method

Setting the target for trimming C_{FY}=0.0179, C_{MX}=0.0, and C_{MZ}=0.0. Figure 4 shows the convergence histories of force, moment and trim variables. It should be mentioned that in this figure the force and moment results used for balance evaluation are solved by unsteady solver, the label "actuator" and "body-fitted" present for the calculation method for Jacobin matrix. It is obvious that if the partial derivative of aerodynamic with respect to control inputs can be solved with actuator model, the calculation cost can be further reduced. Unfortunately, no convergence can be obtained when unsteady aerodynamic model used for balance evaluation and quasi-steady model used for Jacobin calculation, this is mainly due to the slop for aerodynamic prediction of the two different method are not similar, especially when the manipulate variable is close to the target. In other words, when the force and moment results used for balance evaluation are solved by a solver, the same solver must be used for Jacobin matrix calculation. It also can be found in these figures that with the aerodynamic and Jacobin matrix both evaluated by unsteady solver, fast convergence reached only with 1 trim iteration, this is because that the good initial guess which deduced from the trimming loop where aerodynamic and Jacobin matrix both evaluated by quasi-steady model was used for initialization, which speed up the trimming process in the second step.

The $\theta_0 = 7.38^{\circ}$, $\theta_{1c} = 0.39^{\circ}$, $\theta_{1s} = -4.67^{\circ}$ are the results from first trimming loop with

actuator model (the convergence history not be shown here), and $\theta_0 = 8.49^\circ$, $\theta_{1c} = 1.75^\circ$, $\theta_{1s} = -5.04^\circ$ for second trimming loop with unsteady aerodynamic model. figure 5 is the comparison of pitch angel of two steps.

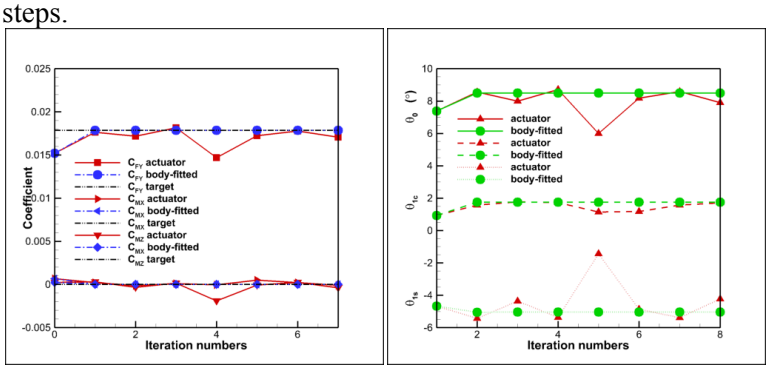

Figure 4: Convergence of aerodynamic and trim variables

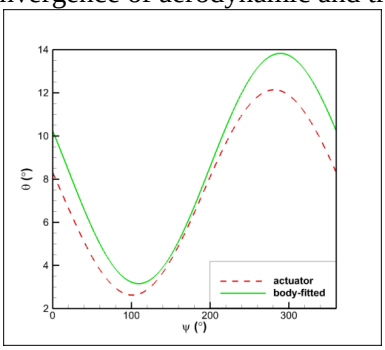

Figure 5: Pitch in 1 rotor revolution

5.22 Single rotor in forward flight with a large shaft angle

Setting the target for trimming C_{FY}=0.00536, C_{FZ}=-0.00536, C_{MX}=0.0 and C_{MZ}=0. The predicted θ_{shaft} is 39.82° with actuator model and θ_{shaft} 39.05° with unsteady aerodynamic model revision. It can be found in figure 6 that 2-3 times iteration is needed for actuator model based trimming process, and 1-2 times iteration for correction with unsteady flow fields simulations.

The predicted $\theta_0 = 17.30^\circ$, $\theta_{1c} = -0.53^\circ$, $\theta_{1s} = -6.54^\circ$ with actuator based trimming loop, and $\theta_0 = 18.99^\circ$, $\theta_{1c} = 1.40^\circ$, $\theta_{1s} = -8.51^\circ$ is the ultimate results with unsteady aerodynamic model. Figure 7 is the predicted pitch with two trimming steps, we find that results discrepancy is a little lager between the two trimming steps when compared with figure 5, this can be explained by the unsteady aerodynamics phenomenon plays an more important role with shaft angle increasing.

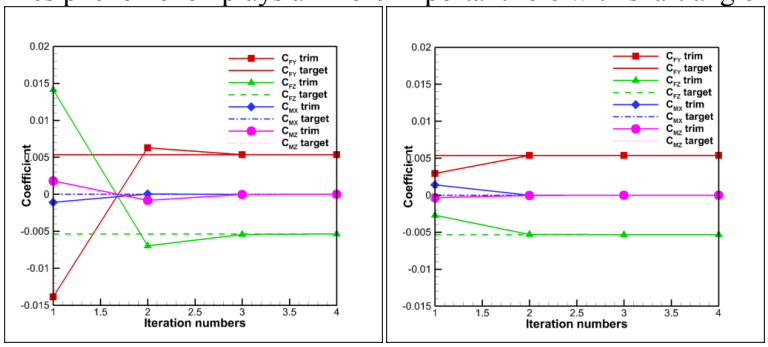

(a) actuator simulation (b) unsteady simulation

Figure 6: Convergence history of force and moment

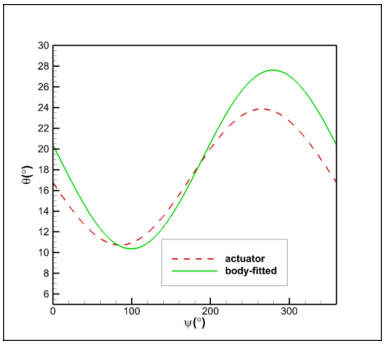

Figure 7: pitch in 1 rotor revolution

5.3 Trimming test cases for complex rotor configuration

5.31 Tilt rotor/nacelle model with a large shaft tilt angle

Tilt rotor model is composed by two nacelles and two rotors, each rotor have 3 blades and the diameter of the rotor is 11.6m, the M_{tip} is 0.68 for rotor in hover state. There is a large, irregular negative twist for rotor blades, the forward flight speed is 30m/s. Setting the target for trimming C_{FY}= 0.015, C_{FZ}=-0.00867, and hub pitching moment C_{MX}=0. Only θ_{shaft} , θ_0, θ_{1c} is need to be determined, θ_{1s} is not be solved as the hub roll moment (C_{Mz}) of one rotor can be balanced by another one.

The convergence histories of the normalized thrust and torque coefficients, trimming variables obtained with the actuator and unsteady flow fields simulation are shown in figure 8 and 9. 2-3 iterations are needed for actuator model, the time consuming can be neglected with the corresponding unsteady method as the algorithms' natural quasi-steady attribution, obtained results are used as initial guess for unsteady simulation, and convergence achieved with 1-2 trim iteration with this input and high computational efficiency achieved.

Figure 10 and 11 are the pressure contour on the rotor and nacelle surface and in flow fields section with actuator simulation. Figure 12 is the schematic of adaptive Cartesian grid sections for unsteady flow fields simulation. Figure 13, 14 give the Vorticity contour of unsteady flow fields.

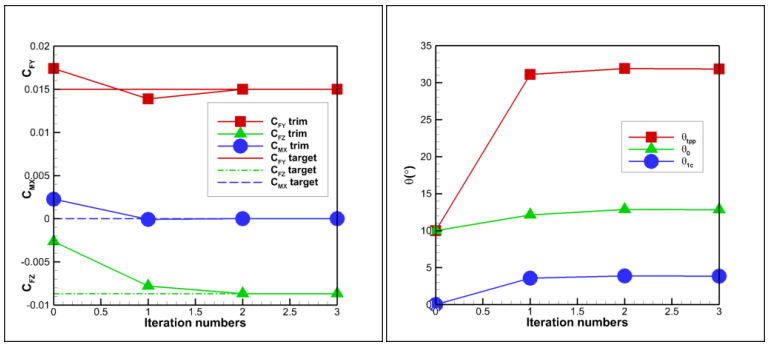

Figure 8: Force, moment, pitch angels trimming results based on actuator model

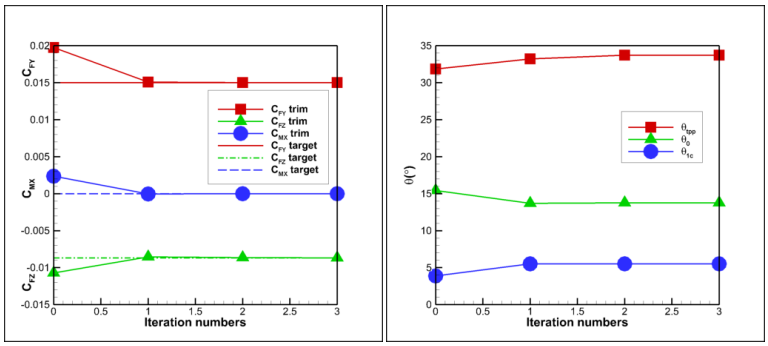

Figure 9: Force, moment, pitch angels trimming results based on unsteady flow fields simulation

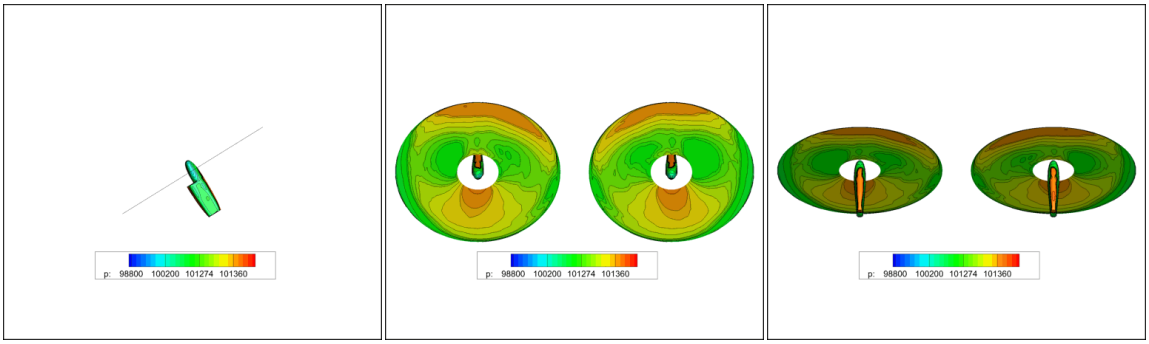

Figure 10: Pressure distributions on the rotor and nacelle surface with actuator simulation

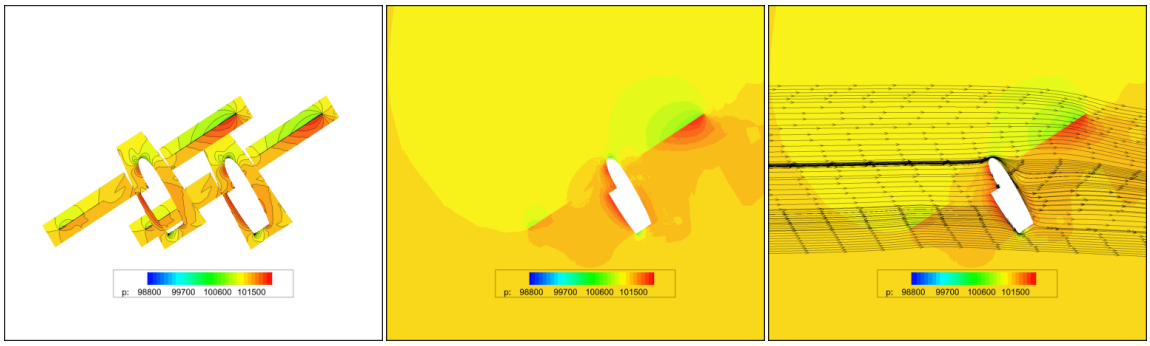

Figure 11: Pressure contours on characteristic flow fields section with actuator simulation

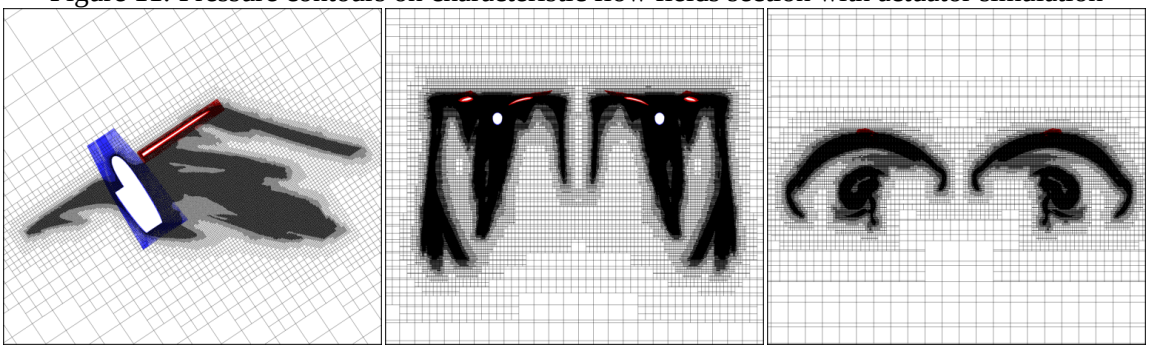

Figure 12: Adaptive Cartesian grid sections for unsteady flow fields simulation

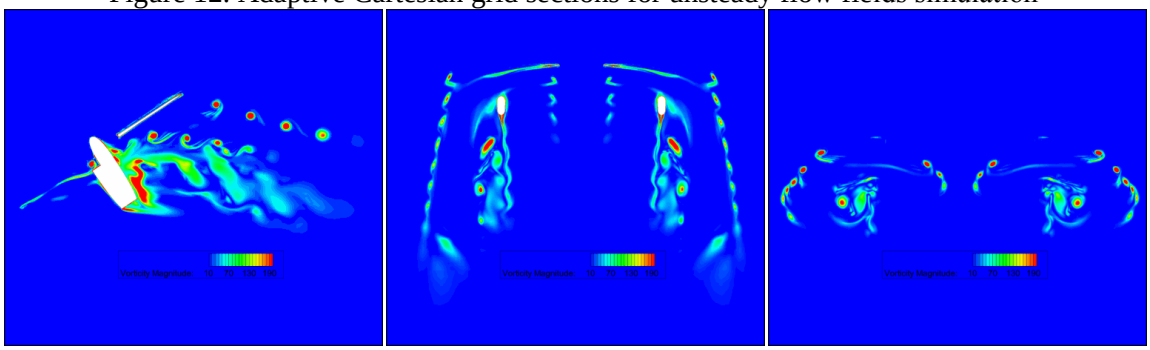

Figure 13: Vorticity contour on flow fields sections with unsteady simulation

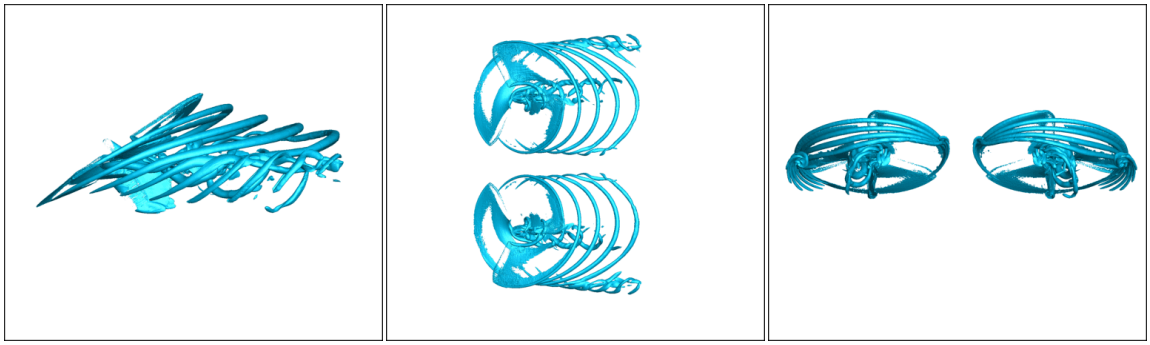

Figure 14: Vorticity ISO-surface of flow fields with unsteady simulation

5.32 Coaxial rotor with a setting frozen parameter

The coaxial rotor model in section 5.12 is used here, for this case M_{tip} in hover is 0.347 and the advanced ratio is 0.169. Setting the target for trimming C_{FX}=0.0, C_{FY}=0.02, C_{FZ}=-0.001889, and C_{MX}=0, C_{MY}=0, C_{MZ}=0. The rotational center coordinate of the upper rotor is (0.0, 0.0, 0.0), the reference coordinate for moment calculation is (0.0, -0.5, 0.0).

For the coaxial rotor in forward flight, same shaft angle is used for upper and lower rotor and the pitch coefficients, 3 undetermined variables for each rotors, consist total 7 variables for 6 balance equations, the θ_{1s} for the lower rotor is frozen as 4° for convenient. Table 1 is the result obtained with two trimming stage. Similar convergence efficiency like above mentioned cases is obtained and not shown here.

Table 1: predicted trimming results for a coaxial in forward flight with 1 frozen parameter

		Upper rotor			Lower rotor		
	θ_{shaft}	θ_0	θ_{1c}	θ_{1s}	θ_0	θ_{1c}	θ_{1s}
Actuator	5.367	10.176	1.305	-4.362	10.202	1.328	4
Unsteady	5.603	11.025	1.846	-4.498	11.056	1.757	4

Figure 15 is the comparison of force and moment results from the two trimming stage, where "initial" means the unsteady aerodynamic results obtained with actuator model trimming variable as input. The ultimate force and moment results show the similar curve shape but a little amplitude discrepancy when compared with the initial results. Figure 16 is the trimmed force and moment for lower and upper rotor in 1 revolution. Figure 17 is the vorticity capture of the flow fields with the refined background grid.

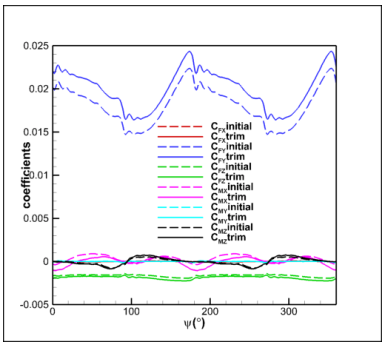

Figure 15: Comparison of force and moment before and after trimming

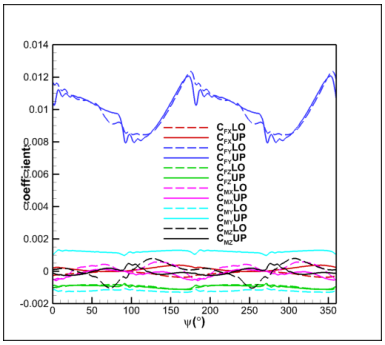

Figure 16: Force and moment in 1 rotor revolution (LO: lower rotor, UP: upper rotor)

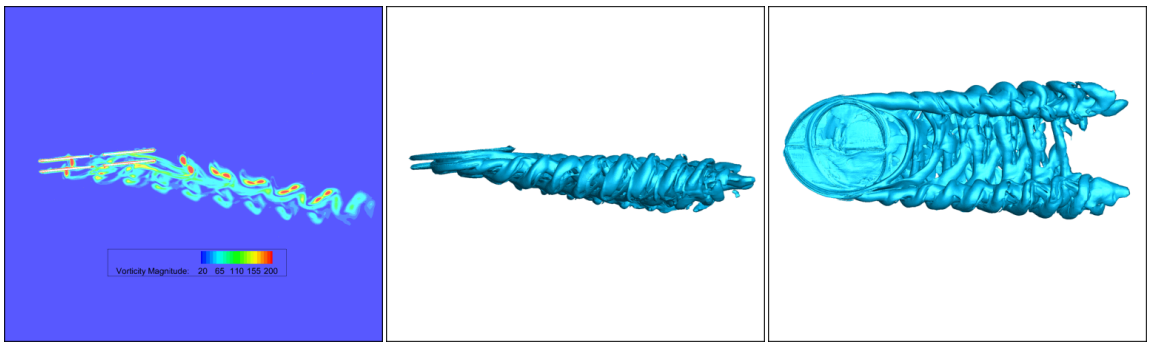

Figure 17: Flow fields of a coaxial rotor in forward flight

6 Conclusion and Future Work

A two-layer trim model was developed for predicting the movement of rotors and blades, a quasi-steady actuator model was used in the first trimming process for both aerodynamic evaluating and Jacobin matrix calculation, the unsteady aerodynamics model which based on blade body-fitted embedded grid was adopted for ultimate control input variables revision. More accuracy trimming results are expected to be obtained as the periodical averaged aerodynamic of unsteady flow fields simulation are used for assessment.

Numerical experiments on a single rotor in forward flight indicates that with the initial guess obtained from the first trimming step, rapid convergence can be obtained for the second stage with unsteady aerodynamic assessment, only 1-2 Newton iteration is needed and the calculation cost is effectively controlled for the times for unsteady flow solver calling is limited. A tilt rotor in conversion mode and a coaxial rotor in forward flight studies also reveal similar characteristics for trimming convergence, which show that present method is also can be applied for trimming simulation for rotorcraft with complex configuration with high efficiency and acceptable numerical accuracy.

Future work includes further improving the numerical accuracy and reducing computational costs, and get the optimal results of a multi-solve questions for rotorcraft with redundant control input.

Acknowledgements

This work is supported by the National key research and development project of China (No. 2016YFB0200903).

References

[1] D. A. Peters and D. Barwey. A general theory of rotorcraft trim. AIAA-95-1451-CP.

[2] D. C. Sekhar and R. Ganguli. Fractal boundaries of basin of attraction of Newton–Raphson method in helicopter trim. Computers and mathematics with applications, 60: 2834–2858, 2010.

[3] S. Gouravaraju and R. Ganguli. Estimating the Hausdorff–Besicovitch dimension of boundary of basin of attraction in helicopter trim. Applied mathematics and computation, 218: 10435–

10442, 2012.
[4] J. Y. Dai, G. H. Wu, Y. H. Wu and G. M. Zhu. Helicopter trim research based on hybrid genetic algorithm. The 7th world congress on intelligent control and automation, Chong Qing, China, 2008.
[5] R. Enns and J. Si. Helicopter trimming and tracking control using direct neural dynamic programming. IEEE transactions on neural networks, 14(4): 929 - 939, 2003.
[6] S. Subramanian, S. Venkataratnam and G. H. Gaonkar. Parallel fast-floquet analysis of trim and stability for large helicopter models. Mathematical and computer modelling, 33: 1155-1176, 2001.
[7] D. C. Sekhar and R. Ganguli. Modified Newton, rank-1 Broyden update and rank-2 BFGS update methods in helicopter trim: A comparative study. Aerospace science and technology, 23: 187–200, 2012.
[8] C. Friedman and O. Rand. Robust trim procedure for rotorcraft configurations. Aerospace science and technology, 45: 442–448, 2015.
[9] W. M. Stumpf and D. A. Peters. An integrated finite-state model for rotor deformation, nonlinear airloads, inflow and trim. Mathl. Comput. modelling. 18(3/4): 115-129, 1993.
[10] J. D. Lee and S. M. Ruffin. Application of a turbulent viscous cartesian-grid methodology to flowfields with rotor-fuselage interaction. AIAA 2007-1280.
[11] M. R. Ruith. Unstructured, multiplex rotor source model with thrust and moment trimming-Fluent's VBM model. AIAA 2005-5217.
[12] R. Steijl, G. N. Barakos and K. J. Badcock. A CFD framework for analysis of helicopter rotors. AIAA 2005-5124.
[13] Z. Yang, L. N. Sankar, M. Smith and O. Bauchau. Recent improvements to a hybrid method for rotors in forward flight. AIAA 2000-0260.
[14] W. L. Lyu and G. H. Xu. New trim method based investigation on the cyclic pitch effected Advancing Blade Concept helicopter Aerodynamics. Journal of aircraft, 52(4): 1365-1371, 2015.
[15] L. Ye, Q. J. Zhao and G. H. Xu. An adaptive unstructured embedded mesh methodology suitable for the calculation on the rotor vortex flowfield. Acta Aerodynamica Sinica, 28(3): 261-266, 2010.
[16] R. G. Rajagopalan and S. R. Mathur. Three dimensional analysis of a rotor in forward flight. Proceedings of 47th Annual forum of American Helicopter Society, 1991.
[17] Y. Zhang, L. Ye and S. Yang. Numerical study on flow fields and aerodynamics of tilt rotor aircraft in conversion mode based on embedded grid and actuator model. Chinese journal of aeronautics, 28(1): 93-102, 2015.
[18] A. Jameson. Time-dependent calculations using multigrid with applications to unsteady flows past airfoils and wings. AIAA 91-1596.
[19] H. Luo and J. D. Baum. A fast, matrix-free implicit method for computing low mach number flows on unstructured grids. AIAA 99-3315.
[20] P. L. Roe. Approximate Riemann solvers, parameter vectors, and difference schemes. Journal of computational physics, 43(2): 357-372, 1981.
[21] V. Venkatakrishnan. On the accuracy of limiters and convergence to steady state solutions. AIAA 93-0880.
[22] P. R. Spalart and S. R. Allmaras. A one-equation turbulence model for aerodynamic flows. AIAA-1992-439.
[23] J. W. Mckee and R. L. Naeseth. Experimental investigation of the drag of flat plates and cylinders in the slipstream of a hovering rotor, NACA TN 4239, 1958.
[24] Z. F. Tang, F. Li, Z. GAO, et al. Measurement of the coaxial-rotor flowfield in hovering using 3-D laser Doppler velocimeter. Experiments and measurements in fluid mechanics, 12(1): 81-87, 1998.
[25] A. Brand, N. M. Komerath and H. M. McMahon. Surface pressure measurements on a body subject to vortex wake interaction. AIAA Journal, 27(5): 569-574, 1989.
[26] F. X. Caradonna and C. Tung. Experimental and analytical studies of a model helicopter rotor in hover. Vertica, 5(1): 149-161, 1981.